Calculation of proton-^{3}He elastic scattering between 7 and 35 MeV

A. Deltuva and A. C. Fonseca
Centro de Física Nuclear da Universidade de Lisboa, P-1649-003 Lisboa, Portugal
(Received 21 March 2013; published 20 May 2013)

Background: Theoretical calculations of the four-particle scattering above the four-cluster breakup threshold are technically very difficult due to nontrivial singularities or boundary conditions. Further complications arise when the long-range Coulomb force is present.
Purpose: We aim at calculating proton-^{3}He elastic scattering observables above three- and four-cluster breakup threshold.
Methods: We employ Alt, Grassberger, and Sandhas (AGS) equations for the four-nucleon transition operators and solve them in the momentum-space framework using the complex-energy method whose accuracy and practical applicability is improved by a special integration method.
Results: Using realistic nuclear interaction models we obtain fully converged results for the proton-^{3}He elastic scattering. The differential cross section, proton and ^{3}He analyzing powers, spin correlation and spin transfer coefficients are calculated at proton energies ranging from 7 to 35 MeV. Effective three- and four-nucleon forces are included via the explicit excitation of a nucleon to a Δ isobar.
Conclusions: Realistic proton-^{3}He scattering calculations above the four-nucleon breakup threshold are feasible. There is quite good agreement between the theoretical predictions and experimental data for the proton-^{3}He scattering in the considered energy regime. The most remarkable disagreements are the peak of the proton analyzing power at lower energies and the minimum of the differential cross section at higher energies. Inclusion of the Δ isobar reduces the latter discrepancy.

DOI: 10.1103/PhysRevC.87.054002 PACS number(s): 21.45.−v, 25.10.+s, 21.30.−x, 24.70.+s

I. INTRODUCTION

Proton-^{3}He (p-^{3}He) scattering is one of the most commonly used experiments to study the four-nucleon system [1]: It involves two charged particles that are stable and easy to detect with acceptable precision, there are no competing channels until $E_p = 7.3$ MeV proton laboratory energy, and beyond that only three- and four-cluster breakup takes place up to the pion-production threshold. Much like neutron-^{3}H (n-^{3}H) scattering, p-^{3}He is dominated by isospin $T = 1$, but has the deciding experimental advantage of having a proton beam and a nonradioactive ^{3}He target. On the contrary, from the theoretical point of view, p-^{3}He is more difficult to calculate than n-^{3}H due to the long-range Coulomb force between protons (p) that gives rise to complicated boundary conditions in the coordinate-space and noncompact kernel in the momentum-space representation. Nevertheless, these difficulties have been solved below the three-cluster breakup threshold using three different theoretical frameworks, namely, the hyperspherical harmonics (HH) expansion method [2,3], the Faddeev-Yakubovsky (FY) equations [4] for the wave function components in coordinate space [5,6], and the Alt, Grassberger, and Sandhas (AGS) equations [7] for transition operators that were solved in the momentum space [8,9]. A good agreement between these methods has been demonstrated in a benchmark for n-^{3}H and p-^{3}He elastic scattering observables [10] using realistic nucleon-nucleon (NN) potentials much like the earlier benchmark [11] proved the accuracy of HH and AGS calculations for p-d elastic scattering.

Recently we extended the AGS calculations to energies above three- and four-cluster breakup thresholds [12,13]. The complex energy method [14,15] was used to deal with the complicated singularities in the four-particle scattering equations; its accuracy and practical applicability was greatly improved by a special integration method [12]. This allowed us to achieve fully converged results for n-^{3}H elastic scattering and neutron-neutron-deuteron recombination into $n + {}^3$H using realistic NN interactions. We note that the FY calculations of n-^{3}H elastic scattering have been recently extended as well to energies above the four-nucleon breakup threshold [16], however, using a semirealistic NN potential limited to S waves.

In the present work we extend the method of Ref. [12] to calculate the p-^{3}He elastic scattering above breakup threshold and compare with existing data for cross sections and spin observables over a wide range of proton beam energies up to $E_p = 35$ MeV. The pp Coulomb interaction is treated as in Refs. [9,17] using the method of screening of the pp Coulomb potential followed by the phase renormalization of transition amplitudes [18,19]. Thus, standard AGS scattering equations with short-range potentials are applicable. At energies bellow three-cluster threshold our results agree with those obtained by other methods as mentioned in Ref. [10]. Compared to our previous n-^{3}H scattering calculations above the breakup threshold [12], the most serious complication for p-^{3}He is the convergence of the partial-wave expansion that requires a larger number of states due to the longer range of the screened Coulomb potential.

In Sec. II we describe the theoretical formalism and in Sec. III we present the numerical results. The summary is given in Sec. IV.

II. 4N SCATTERING EQUATIONS

We use the symmetrized AGS equations [8] as appropriate for the four-nucleon system in the isospin formalism. They

are integral equations for the four-particle transition operators $\mathcal{U}_{\beta\alpha}$, i.e.,

$$\mathcal{U}_{11} = -(G_0\, t G_0)^{-1} P_{34} - P_{34} U_1 G_0\, t G_0\, \mathcal{U}_{11} + U_2 G_0\, t G_0\, \mathcal{U}_{21}, \quad (1a)$$

$$\mathcal{U}_{21} = (G_0\, t\, G_0)^{-1}(1 - P_{34}) + (1 - P_{34}) U_1 G_0\, t\, G_0\, \mathcal{U}_{11}. \quad (1b)$$

Here, $\alpha = 1$ corresponds to the $3 + 1$ partition (12,3)4 whereas $\alpha = 2$ corresponds to the $2 + 2$ partition (12)(34); there are no other distinct two-cluster partitions in the system of four identical particles. The free resolvent at the complex energy $E + i\varepsilon$ is given by

$$G_0 = (E + i\varepsilon - H_0)^{-1}, \quad (2)$$

with H_0 being the free Hamiltonian. The pair (12) transition matrix

$$t = v + v G_0 t \quad (3)$$

is derived from the potential v; for the pp pair v includes both the nuclear and the screened Coulomb potential w_R. Our calculations are done in momentum space; however, we start with the configuration-space representation

$$w_R(r) = w(r)\, e^{-(r/R)^n}, \quad (4)$$

where $w(r) = \alpha_e/r$ is the true Coulomb potential, $\alpha_e \simeq 1/137$ is the fine structure constant, R is the screening radius, and n controls the smoothness of the screening. All transition operators acquire parametric dependence on R but it is suppressed in our notation, except for the scattering amplitudes. The symmetrized $3 + 1$ or $2 + 2$ subsystem transition operators are obtained from the respective integral equations

$$U_\alpha = P_\alpha G_0^{-1} + P_\alpha t\, G_0\, U_\alpha. \quad (5)$$

The basis states are antisymmetric under exchange of two particles in the subsystem (12) for the $3 + 1$ partition and in subsystems (12) and (34) for the $2 + 2$ partition. The full antisymmetry of the four-nucleon system is ensured by the permutation operators P_{ab} of particles a and b with $P_1 = P_{12}\, P_{23} + P_{13}\, P_{23}$ and $P_2 = P_{13}\, P_{24}$.

The p-^{3}He scattering amplitude with nuclear plus screened Coulomb interactions at available energy $E = \epsilon_1 + 2p_1^2/3m_N$ is obtained from the on-shell matrix element $\langle \mathbf{p}_1' | T_{(R)} | \mathbf{p}_1 \rangle = 3\langle \phi_1' | \mathcal{U}_{11} | \phi_1 \rangle$ in the limit $\varepsilon \to +0$. Here $|\phi_1\rangle$ is the Faddeev component of the asymptotic p-^{3}He state in the channel $\alpha = 1$, characterized by the bound state energy $\epsilon_1 = -7.72$ MeV and the relative p-^{3}He momentum $\mathbf{p}_1$, m_N being the average nucleon mass. Due to energy conservation $p_1' = p_1$.

The amplitude $\langle \mathbf{p}_1' | T_{(R)} | \mathbf{p}_1 \rangle$ is decomposed into its long-range part $\langle \mathbf{p}_1' | t_R^{\rm c.m.} | \mathbf{p}_1 \rangle$, being the two-body on-shell transition matrix derived from the screened Coulomb potential of the form (4) between the proton and the center of mass (c.m.) of ^{3}He, and the remaining Coulomb-distorted short-range part. Renormalizing $\langle \mathbf{p}_1' | T_{(R)} | \mathbf{p}_1 \rangle$ by the phase factor Z_R^{-1} [9,18,19], in the $R \to \infty$ limit, yields the full p-^{3}He transition amplitude in the presence of Coulomb

$$\langle \mathbf{p}_1' | T | \mathbf{p}_1 \rangle = \langle \mathbf{p}_1' | t_C^{\rm c.m.} | \mathbf{p}_1 \rangle + \lim_{R\to\infty} \left\{ \langle \mathbf{p}_1' | \left[T_{(R)} - t_R^{\rm c.m.} \right] | \mathbf{p}_1 \rangle Z_R^{-1} \right\}, \quad (6)$$

where the first term is obtained from $Z_R^{-1} \langle \mathbf{p}_1' | t_R^{\rm c.m.} | \mathbf{p}_1 \rangle$ that converges, in general as a distribution, to the exact Coulomb amplitude $\langle \mathbf{p}_1' | t_C^{\rm c.m.} | \mathbf{p}_1 \rangle$ between the proton and the c.m. of the ^{3}He nucleus [19]. The renormalization factor Z_R is defined in Refs. [9,17]. The second term in Eq. (6), after renormalization by Z_R^{-1}, represents the Coulomb-modified nuclear short-range amplitude. It has to be calculated numerically, but, due to its short-range nature, the $R \to \infty$ limit is reached with sufficient accuracy at finite screening radii R. Since the convergence with R is faster at higher energies, the required screening radii are smaller than in our low-energy p-^{3}He calculations [9]. We found that R ranging from 8 to 10 fm leads to well-converged results in the energy regime considered in the present paper. Furthermore, we take a sharper screening with $n = 6$ such that at short distances $r < R$ the screened Coulomb approximates the full Coulomb better than with $n = 4$ used in Ref. [9] and at the same time vanishes more rapidly at $r > R$ thereby accelerating the partial-wave convergence.

We solve the AGS equations (1) in the momentum-space partial-wave framework. The states of the total angular momentum $\mathcal{J}$ with the projection $\mathcal{M}$ are defined as $|k_x\, k_y\, k_z [l_z (\{ l_y [(l_x S_x) j_x\, s_y] S_y \} J_y s_z) S_z]\, \mathcal{J}\mathcal{M}\rangle$ for the $3 + 1$ configuration and $|k_x\, k_y\, k_z (l_z \{ (l_x S_x) j_x\, [l_y (s_y s_z) S_y] j_y \} S_z) \mathcal{J}\mathcal{M}\rangle$ for the $2 + 2$. Here k_x, k_y and k_z are the four-particle Jacobi momenta in the convention of Ref. [20], l_x, l_y, and l_z are the associated orbital angular momenta, j_x and j_y are the total angular momenta of pairs (12) and (34), J_y is the total angular momentum of the (123) subsystem, s_y and s_z are the spins of nucleons 3 and 4, and S_x, S_y, and S_z are channel spins of two-, three-, and four-particle system. A similar coupling scheme is used for the isospin. We include a large number of four-nucleon partial waves, up to $l_x, l_y, l_z, j_x, j_y = 7$, $J_y = \frac{13}{2}$, and $\mathcal{J} = 6$, such that the results are well converged. In fact, lower cutoffs are sufficient for

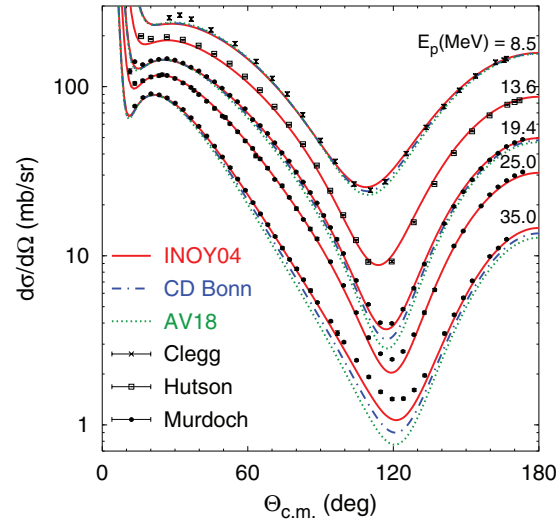

FIG. 1. (Color online) Differential cross section for elastic p-^{3}He scattering at 8.52, 13.6, 19.4, 25.0, and 35.0 MeV proton energy as function of the c.m. scattering angle. Results obtained with INOY04 (solid curves), and, at selected energies, with CD-Bonn (dashed-dotted curves) and AV18 (dotted curves) potentials are compared with the experimental data from Refs. [25–27].

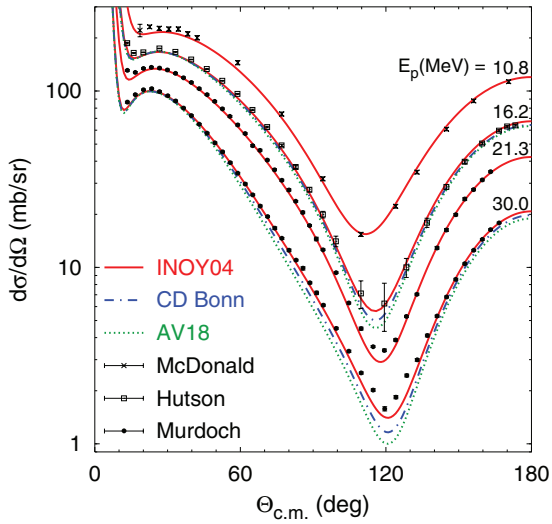

FIG. 2. (Color online) Same as in Fig. 1 but at 10.77, 16.23, 21.3, and 30.0 MeV proton energy. The experimental data are from Refs. [26–28].

lower $\mathcal{J}$, e.g., $l_x, l_y, l_z, j_x, j_y \leqslant 5$ and $J_y \leqslant \frac{9}{2}$ are sufficient for $\mathcal{J} \leqslant 3$. Furthermore, for most observables $\mathcal{J} \leqslant 5$ or even $\mathcal{J} \leqslant 4$ are enough for the convergence; $\mathcal{J} = 6$ yields small but still visible effect only above $E_p = 30$ MeV.

The numerical calculations are performed for complex energies, i.e., with finite ε. The limit $\varepsilon \to +0$ needed for the calculation of the amplitude $\langle \mathbf{p}_1' | T_{(R)} | \mathbf{p}_1 \rangle$ is obtained by the extrapolation of finite ε results as proposed in Ref. [14]. A special integration method developed in Ref. [12] is used to treat the quasisingularities of the AGS equations (1). We obtain accurate results by using ε ranging from 1 to 2 MeV at lowest considered energies and from 2 to 4 MeV at highest considered energies. Grid points for the discretization of each momentum variable range from 30 (at lower energies) to 35 (at higher energies). Further details on the other numerical techniques for solving the four-nucleon AGS equations can be found in Ref. [8].

III. RESULTS

We study the p-^{3}He scattering using realistic high-precision NN potentials, namely, the Argonne (AV18) potential [21], the inside-nonlocal outside-Yukawa (INOY04) potential by Doleschall [5,22], the charge-dependent Bonn potential (CD-Bonn) [23], and its extension CD-Bonn + Δ [24] allowing for an excitation of a nucleon to a Δ isobar and thereby yielding effective three- and four-nucleon forces (3NF and 4NF). The ^{3}He binding energy calculated with AV18, CD-Bonn, CD-Bonn + Δ, and INOY04 potentials is 6.92, 7.26, 7.54, and 7.73 MeV, respectively; the experimental value is 7.72 MeV. Therefore most of our predictions correspond to INOY04 as it is the only potential that nearly reproduces the experimental binding energy of ^{3}He. The calculations with other potentials are done at fewer selected energies.

In Figs. 1 and 2 we show the differential cross section $d\sigma/d\Omega$ for elastic p-^{3}He scattering as a function of the c.m. scattering angle $\Theta_{\text{c.m.}}$ at a number of proton energies ranging from $E_p = 8.5$ to 35.0 MeV. This observable decreases rapidly with the increasing energy and also changes the shape; the

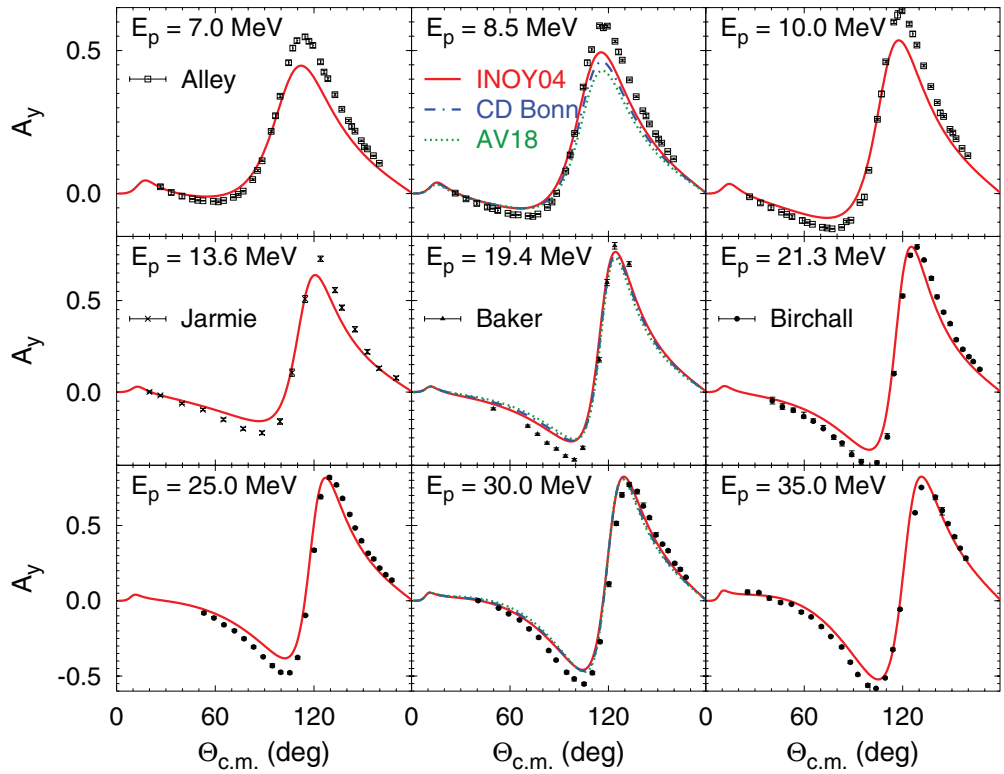

FIG. 3. (Color online) Proton analyzing power A_y for elastic p-^{3}He scattering at 7.03, 8.52, 10.03, 13.6, 19.4, 21.3, 25.0, 30.0, and 35.0 MeV proton energy. Curves as in Fig. 1. The experimental data are from Refs. [31–34].

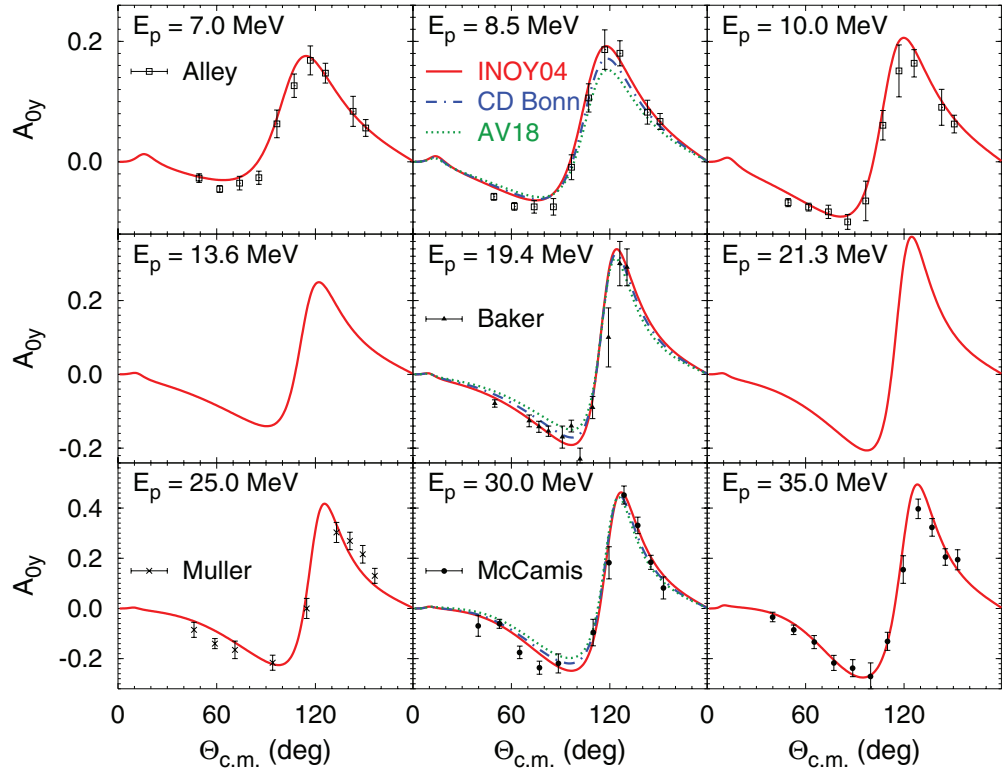

FIG. 4. (Color online) ^{3}He analyzing power A_{0y} for elastic p-^{3}He scattering at 7.03, 8.52, 10.03, 13.6, 19.4, 21.3, 25.0, 30.0, and 35.0 MeV proton energy. Curves as in Fig. 1. The experimental data are from Refs. [31,33,37,38].

calculations describe the energy and angular dependence of the experimental data fairly well. Below $E_p = 15$ MeV the experimental data are slightly underpredicted at forward angles as happens also at energies below the three-cluster breakup threshold [9,10]. At the minimum the $d\sigma/d\Omega$ predictions scale with the ^{3}He binding energy: the weaker the ^{3}He binding the lower the dip of $d\sigma/d\Omega$ that is located between $\Theta_{\rm c.m.} = 105^\circ$ and $\Theta_{\rm c.m.} = 125^\circ$. The scaling is more pronounced at higher E_p. For the INOY04 potential that fits the ^{3}He binding energy, one gets an good agreement in the whole angular region up to $E_p \simeq 20$ MeV but, as the energy increases, the calculated cross section underpredicts the data at the minimum much like what happens in nucleon-deuteron elastic scattering [17,29,30] but for nucleon energies above 60 MeV. In line with the conjectures that were made 15 years ago for the three-nucleon system [29,30], this underprediction of the data at the minimum of $d\sigma/d\Omega$ may be a sign for the need to include the 3NF.

In Fig. 3 we show the proton analyzing power A_y for elastic p-^{3}He scattering at proton energies ranging from 7.0 to 35.0 MeV. We observe that the sensitivity to the nuclear force model and energy is considerably weaker as compared to the regime below three-cluster threshold [8,9]. Most remarkably, in contrast to low energies where the famous p-^{3}He A_y-puzzle exists [2,9,35], the peak of A_y around 120 degrees is described fairly well but there is a discrepancy in the minimum region. This is similar to the energy evolution of the A_y-puzzle in p-d elastic scattering [36]. Consistently with findings of Ref. [36], at lower energies the proton analyzing power A_y is dominated by p-^{3}He P waves but with increasing energy also D and F waves become important.

In Fig. 4 we show the ^{3}He analyzing power A_{0y} for elastic p-^{3}He scattering at proton energies ranging from 7.0 to 35.0 MeV. A_{0y} varies slowly with energy but is slightly more sensitive to the NN potential. Contrary to A_y, calculated A_{0y} is in better agreement with data over the whole energy range, particularly when the INOY04 potential is used.

The experimental data are scarcer for double polarization observables. In Fig. 5 we show the p-^{3}He spin correlation

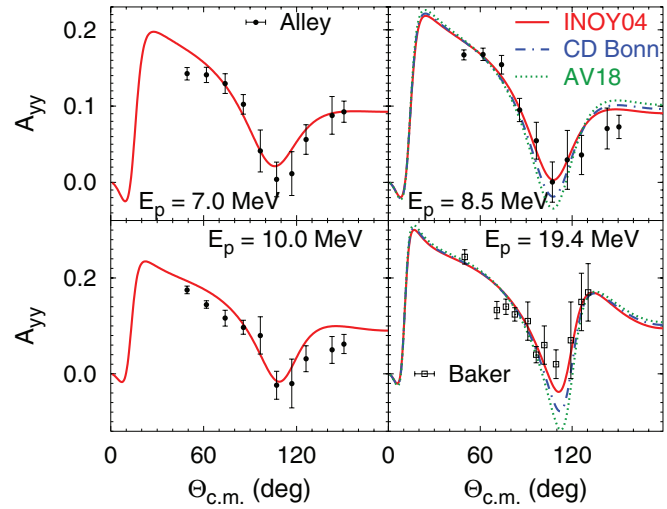

FIG. 5. (Color online) p-^{3}He spin correlation coefficient A_{yy} for elastic p-^{3}He scattering at 7.03, 8.52, 10.03, and 19.4 MeV proton energy. Curves as in Fig. 1. The experimental data are from Refs. [31,33].

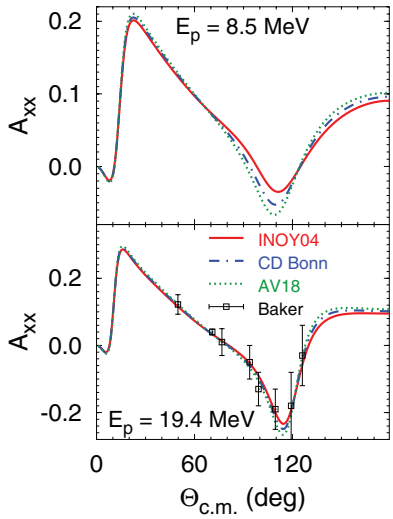

FIG. 6. (Color online) p-^{3}He spin correlation coefficient A_{xx} for elastic p-^{3}He scattering at 8.52 and 19.4 MeV proton energy. Curves as in Fig. 1. The experimental data are from Ref. [33].

coefficient A_{yy} for elastic p-^{3}He scattering at 7.03, 8.52, 10.03, and 19.4 MeV, and in Fig. 6 we show A_{xx} for elastic p-^{3}He scattering at 8.52 and 19.4 MeV proton energy. Calculated A_{yy} exhibits some sensitivity to the NN potential model and describes the data reasonably well; the agreement with data is the best when the INOY04 interaction is used. The same happens for A_{xx} but for the single data set we know of.

Finally in Fig. 7 we show the proton spin transfer coefficients $K_x^{x'}$, $K_z^{x'}$, and $K_y^{y'}$ for elastic p-^{3}He scattering at 8.52, 10.77, and 16.23 MeV proton energy. Note that 8.52-MeV predictions are compared to experimental data taken at 8.82 MeV but, given the weak energy dependence of these observables, the comparison is appropriate. The calculated spin transfer coefficients show a rich angular structure and follow the data reasonably well but cannot be fully tested by the available data confined to the angular region below $\Theta_{\text{c.m.}} = 110^\circ$. In contrast to other shown spin observables, the spin transfer coefficient $K_z^{x'}$ around $\Theta_{\text{c.m.}} = 120^\circ$, i.e., in the region of the differential cross section minimum, varies quite rapidly with the energy. There is little sensitivity to NN interaction model, except for $K_y^{y'}$ around $\Theta_{\text{c.m.}} = 120^\circ$ at $E_p = 16.23$ MeV. Theoretical results and experimental data for $K_y^{y'}$ are close to 1 up to $\Theta_{\text{c.m.}} = 90^\circ$, but data sets at different energies seem to be inconsistent as they show different angular dependence. In contrast, theoretical predictions at the three considered energies show nearly the same angular dependence for $\Theta_{\text{c.m.}} \leqslant 90^\circ$.

As already mentioned, above $E_p = 20$ MeV the minimum of the elastic differential cross section is underpredicted. In order to establish the importance of the 3NF as a means to cure this discrepancy we study the effect of the Δ-isobar excitation on both the differential cross section and proton analyzing power at 30 MeV proton energy. This has been done before at energies below three-cluster breakup threshold [41] and we follow here the same procedure. The results are shown in Fig. 8 in a way that one can single out the Δ-isobar effects

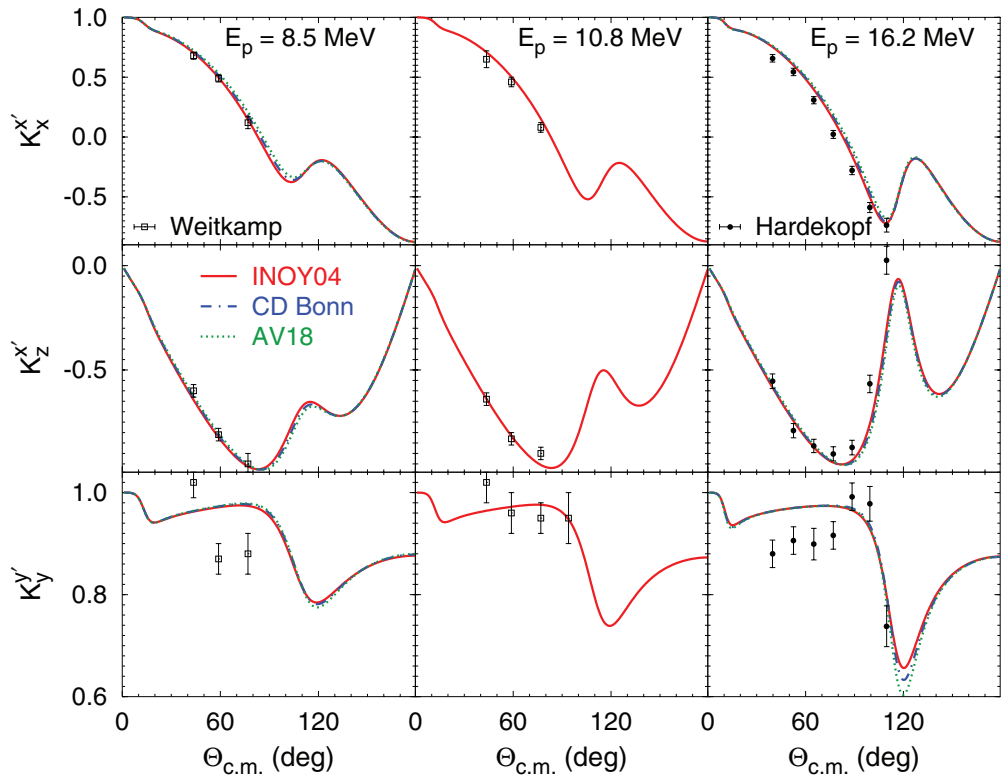

FIG. 7. (Color online) Proton spin transfer coefficients $K_x^{x'}$, $K_z^{x'}$, and $K_y^{y'}$ for elastic p-^{3}He scattering at 8.52, 10.77, and 16.23 MeV proton energy. Curves as in Fig. 1. The experimental data are from Refs. [39,40].

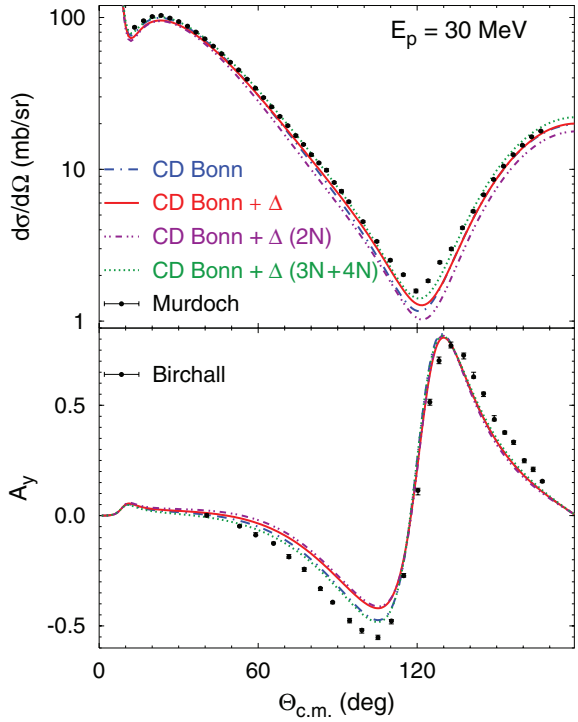

FIG. 8. (Color online) Differential cross section and proton analyzing power A_y for elastic p-^{3}He scattering at 30 MeV proton energy. Results obtained with CD-Bonn (dashed-dotted curves) and CD-Bonn + Δ (solid curves) potentials are compared with the experimental data from Refs. [27,34]. In addition are shown the predictions including Δ effects of $2N$ nature (dashed-double-dotted curves) and of $3N$ and $4N$ nature (dotted curves).

of $2N$ nature, the so-called $2N$ dispersion, and of $3N$ and $4N$ nature, the 3NF and 4NF. The competition between $2N$ dispersion and 3NF, often found in the $3N$ system, is well seen also here for the differential cross section. As shown in Fig. 8 dispersive effect increases the discrepancy with data (dashed-double dotted curves) while 3NF and 4NF effects reverse that trend for the differential cross section (dotted curves). Nevertheless, when the two effects are put together the net result is an improvement towards the data (solid curves) but not quite enough to bridge the original gap. For A_y only the dispersive effect around the minimum is visible; it moves the predictions away from data.

IV. SUMMARY

In summary, we performed fully converged proton-^{3}He elastic scattering calculations with realistic potentials above the three- and four-cluster breakup threshold. The symmetrized Alt, Grassberger, and Sandhas four-particle equations were solved in the momentum-space framework. We used the complex energy method whose accuracy and efficiency is greatly improved by the numerical integration technique with special weights. The pp Coulomb interaction was included rigorously using the method of screening and renormalization.

The differential cross section exhibits rapid energy dependence and, in the minimum region around $\Theta_{\rm c.m.} = 120^\circ$, also sensitivity to the NN interaction model. The calculations using the INOY04 potential describe the experimental data well up to $E_p = 20$ MeV but underpredict the differential cross section in the minimum at higher energies; other potential models fail even more. In contrast, most of the calculated spin observables show little sensitivity to the interaction model, and also the dependence on the beam energy is weaker than below the three-cluster breakup threshold. The overall agreement with the experimental data for the spin observables is quite good, considerably better than in the low-energy p-^{3}He scattering which is affected by P-wave resonances. In particular, the peak of the proton analyzing power A_y that is strongly underpredicted at low energies, is reproduced fairly well above $E_p = 20$ MeV but there is discrepancy in the minimum. The observed sensitivity to the NN interaction model seems to be mostly due to different predictions of the ^{3}He binding energy; the calculations using the INOY04 potential with correct ^{3}He binding provide the best description of the experimental data.

We also studied the effect of three- and four-nucleon forces through the explicit inclusion of the Δ-isobar excitation. We found that Δ-generated many-nucleon forces significantly improve the description of the differential cross section but have almost no effect for the proton analyzing power. However, there are also quite strong dispersive Δ-isobar effects that often reduce or even reverse the effect of 3NF. Therefore the total Δ-isobar effect, although beneficial, is not large enough to bridge the gap between the differential cross section data and calculations. It even increases the discrepancy in the minimum of A_y. It might be possible that using the standard approach of including static 3NF one might be able to explain the data at higher energies, particularly using effective field theory generated interactions [42,43]. Extension of the method to other reactions in the four-nucleon system is in progress.

[1] D. R. Tilley, H. Weller, and G. M. Hale, Nucl. Phys. A **541**, 1 (1992).
[2] M. Viviani, A. Kievsky, S. Rosati, E. A. George, and L. D. Knutson, Phys. Rev. Lett. **86**, 3739 (2001).
[3] A. Kievsky, S. Rosati, M. Viviani, L. E. Marcucci, and L. Girlanda, J. Phys. G **35**, 063101 (2008).
[4] O. A. Yakubovsky, Yad. Fiz. **5**, 1312 (1967) [Sov. J. Nucl. Phys. **5**, 937 (1967)].
[5] R. Lazauskas and J. Carbonell, Phys. Rev. C **70**, 044002 (2004).
[6] R. Lazauskas, Phys. Rev. C **79**, 054007 (2009).
[7] P. Grassberger and W. Sandhas, Nucl. Phys. B **2**, 181 (1967); E. O. Alt, P. Grassberger, and W. Sandhas, JINR Report No. E4-6688 (1972).
[8] A. Deltuva and A. C. Fonseca, Phys. Rev. C **75**, 014005 (2007).
[9] A. Deltuva and A. C. Fonseca, Phys. Rev. Lett. **98**, 162502 (2007).
[10] M. Viviani, A. Deltuva, R. Lazauskas, J. Carbonell, A. C. Fonseca, A. Kievsky, L. E. Marcucci, and S. Rosati, Phys. Rev. C **84**, 054010 (2011).
[11] A. Deltuva, A. C. Fonseca, A. Kievsky, S. Rosati, P. U. Sauer, and M. Viviani, Phys. Rev. C **71**, 064003 (2005).

[12] A. Deltuva and A. C. Fonseca, Phys. Rev. C **86**, 011001(R) (2012).
[13] A. Deltuva and A. C. Fonseca, Phys. Rev. C **87**, 014002 (2013).
[14] H. Kamada, Y. Koike, and W. Glöckle, Prog. Theor. Phys. **109**, 869L (2003).
[15] E. Uzu, H. Kamada, and Y. Koike, Phys. Rev. C **68**, 061001(R) (2003).
[16] R. Lazauskas, Phys. Rev. C **86**, 044002 (2012).
[17] A. Deltuva, A. C. Fonseca, and P. U. Sauer, Phys. Rev. C **71**, 054005 (2005).
[18] E. O. Alt and W. Sandhas, Phys. Rev. C **21**, 1733 (1980).
[19] J. R. Taylor, Nuovo Cimento B **23**, 313 (1974); M. D. Semon and J. R. Taylor, Nuovo Cimento A **26**, 48 (1975).
[20] A. Deltuva, Phys. Rev. A **85**, 012708 (2012).
[21] R. B. Wiringa, V. G. J. Stoks, and R. Schiavilla, Phys. Rev. C **51**, 38 (1995).
[22] P. Doleschall, Phys. Rev. C **69**, 054001 (2004).
[23] R. Machleidt, Phys. Rev. C **63**, 024001 (2001).
[24] A. Deltuva, R. Machleidt, and P. U. Sauer, Phys. Rev. C **68**, 024005 (2003).
[25] T. B. Clegg, A. C. L. Barnard, J. B. Swint, and J. L. Weil, Nucl. Phys. **50**, 621 (1964).
[26] R. L. Hutson, N. Jarmie, J. L. Detch, and J. H. Jett, Phys. Rev. C **4**, 17 (1971).
[27] B. T. Murdoch, D. K. Hasell, A. M. Sourkes, W. T. H. van Oers, P. J. T. Verheijen, and R. E. Brown, Phys. Rev. C **29**, 2001 (1984).
[28] D. G. McDonald, W. Haeberli, and L. W. Morrow, Phys. Rev. **133**, B1178 (1964).
[29] H. Witała, W. Glöckle, D. Hüber, J. Golak, and H. Kamada, Phys. Rev. Lett. **81**, 1183 (1998).
[30] S. Nemoto, K. Chmielewski, S. Oryu, and P. U. Sauer, Phys. Rev. C **58**, 2599 (1998).
[31] M. T. Alley and L. D. Knutson, Phys. Rev. C **48**, 1890 (1993).
[32] N. Jarmie and J. H. Jett, Phys. Rev. C **10**, 57 (1974).
[33] S. D. Baker, T. Cahill, P. Catillon, J. Durand, and D. Garreta, Nucl. Phys. A **160**, 428 (1971).
[34] J. Birchall, W. T. H. van Oers, J. W. Watson, H. E. Conzett, R. M. Larimer, B. Leemann, E. J. Stephenson, P. von Rossen, and R. E. Brown, Phys. Rev. C **29**, 2009 (1984).
[35] B. M. Fisher, C. R. Brune, H. J. Karwowski, D. S. Leonard, E. J. Ludwig, T. C. Black, M. Viviani, A. Kievsky, and S. Rosati, Phys. Rev. C **74**, 034001 (2006).
[36] A. Kievsky, M. Viviani, and S. Rosati, Phys. Rev. C **64**, 024002 (2001).
[37] D. Müller, R. Beckmann, and U. Holm, Nucl. Phys. A **311**, 1 (1978).
[38] R. H. McCamis, P. J. T. Verheijen, W. T. H. van Oers, P. Drakopoulos, C. Lapointe, G. R. Maughan, N. T. Okumusoglu, and R. E. Brown, Phys. Rev. C **31**, 1651 (1985).
[39] W. Weitkamp, W. Grüebler, V. König, P. Schmelzbach, R. Risler, and B. Jenny, Nucl. Phys. A **311**, 29 (1978).
[40] R. A. Hardekopf and D. D. Armstrong, Phys. Rev. C **13**, 900 (1976).
[41] A. Deltuva, A. C. Fonseca, and P. U. Sauer, Phys. Lett. B **660**, 471 (2008).
[42] E. Epelbaum, W. Glöckle, and U.-G. Meissner, Nucl. Phys. A **671**, 295 (2000).
[43] R. Machleidt and D. R. Entem, Phys. Rep. **503**, 1 (2011).